Urania
Jurnal Ilmiah Daur Bahan Bakar Nuklir

Beranda jurnal: https://ejournal.brin.go.id/urania

A REVIEW ON HIGH-TEMPERATURE STEAM OXIDATION RESISTANCE OF ZIRCONIUM CLADDING MATERIALS SUBJECTED TO PLASMA ELECTROLYSIS

Nisa Nashrah[1], Cahya Krisnawati Marbun[2], Akbar Ridho Saputra[3], Juan Carlos Sihotang[4*]
[1]Department of Physics, Faculty of Mathematics and Natural Sciences, Universitas Indonesia, Depok, Jawa Barat 16424
[2]Department of Chemistry, Faculty of Mathematics and Natural Sciences, Universitas Negeri Surabaya, Surabaya, Jawa Timur 60231
[3]Department of Nuclear Chemical Engineering, Polytechnic Institute of Nuclear Technology, Sleman, Yogyakarta 55281
[4]Research Center for Nuclear Material and Radioactive Waste Technology – BRIN
K.S.T. B.J. Habibie, Bdg. 720, Serpong, Tangerang Selatan, Banten 15314
e-mail: juan004@brin.go.id

(Submitted: 17–07–2025, Revised: 29–09–2025, Accepted: 13–10–2025)

ABSTRACT

A REVIEW ON HIGH-TEMPERATURE STEAM OXIDATION RESISTANCE OF ZIRCONIUM CLADDING MATERIALS SUBJECTED TO PLASMA ELECTROLYSIS. Zirconium alloys, such as Zircaloy-4 and ZIRLO, are the standard cladding materials in pressurized water reactors (PWR) due to their low neutron absorption and corrosion resistance. Yet, under loss-of-coolant accident conditions, rapid steam oxidation above 900 °C accelerates hydrogen uptake, embrittlement, and cladding failure. Plasma electrolysis (PE) has emerged as a promising surface modification strategy, directly converting the Zr surface into a ZrO_2-based ceramic layer with strong adhesion, phase stability, and enhanced oxidation resistance. This review provides a comprehensive overview of PE coating formation, emphasizing anodic oxidation, plasma microdischarge, and incorporation of electrolyte-derived elements that tailor microstructure and tetragonal ZrO_2 stabilization. Comparative assessments show that PE-coated claddings delay breakaway oxidation, suppress oxygen diffusion, and maintain structural integrity better than bare alloys or many physical vapor–deposited coatings. The influence of coolant chemistry, irradiation effects, and thermal cycling on long-term coating durability is also evaluated. Remaining challenges include controlling thickness, mitigating phase transformation, and ensuring irradiation stability. Addressing these issues will be critical to realizing PE-coated zirconium as a viable accident-tolerant fuel cladding for advanced nuclear reactors.

Keywords: Pressurized Water Reactor, cladding materials, zirconium alloys, plasma electrolysis, steam oxidation resistance.

INTRODUCTION

Zirconium (Zr) alloys (e.g., Zircaloy-4, ZIRLO) serve as the primary cladding material in water-cooled nuclear reactors due to their exceptional combination of low thermal neutron absorption cross-section, mechanical strength, and corrosion resistance in high-temperature aqueous environments. As the first barrier to the release of radioactive fission products to the coolant, the integrity of the cladding is critical to ensuring the safe operation of nuclear reactors. However, a major concern during reactor operation is the corrosion of Zr in water, which results in the generation of hydrogen gas. A portion of this hydrogen is absorbed into the Zr alloy, a phenomenon known as hydrogen pickup. When the hydrogen concentration exceeds the solubility limit in the metal, Zr hydride (ZrH_x) precipitates form within the cladding [1]. These hydrides are brittle and significantly degrade the mechanical properties of the material. Moreover, under accident conditions, such as loss-of-coolant accidents (LOCA), cladding temperatures can reach over 1000°C [2]. This steam oxidation generates brittle zirconium oxide (ZrO_2) scales and releases hydrogen, which further embrittles the material through hydride formation (ZrH) [3], [4]. The resulting degradation compromises cladding integrity, posing significant safety risks. Mitigation strategies for cladding include replacing Zr with alternative materials or applying surface modifications to existing Zr-based claddings [5], [6]. Since Zr replacement requires significant changes to reactor core design, surface modification is considered the more practical and preferred option [6], [7].

Several surface modification techniques, including physical vapor deposition (PVD) and spraying (laser spraying and cold spraying) have been investigated for Zr cladding [8]. However, these often suffer from drawbacks like non-uniform coverage (e.g., line-of-sight PVD), low deposition rate (only a few micrometers per hour), the need for complex equipment, poor adhesion and loose structure, high residual stress, and brittle interfacial phases. These flaws make such coatings susceptible to crack initiation and spallation under operational thermal cycling. In contrast, plasma electrolytic oxidation or shortly plasma electrolysis (PE), an electrochemical surface treatment that creates dense adherent ceramic coatings offers promising solution. PE grows primarily tetragonal ZrO_2 *in situ* on Zr alloys, forming a strong metallurgical bond with a gradual interface and a compatible thermal expansion coefficient. [9], [10] This inherent structure grants PE coatings exceptional resistance to thermal cycling-induced delamination, a critical advantage for reactor performance. The PE coatings also exhibit enhanced phase stability (retention of tetragonal ZrO_2 at high temperatures), tailored porosity and chemical composition (e.g., incorporation of Si, Al, or Y to suppress crack propagation) [11], [12], [13]. These characteristics enable PE-coated Zr alloy to resist high-temperature steam corrosion, hydrogen uptake, and thermal shock-key challenges in LOCA scenarios.

Several studies have demonstrated that PE-coated Zr alloys exhibit significantly enhanced corrosion resistance compared to bare Zr when exposed to high-temperature oxidative environments typical of pressurized water reactors (PWR). The PE process forms a dual-layered ZrO_2-based ceramic coating with a dense inner barrier and a porous outer layer, which acts as an effective diffusion barrier against oxidizing species. Surface characterizations after exposure to simulated LOCA or steam oxidation tests at temperatures above 900 °C reveal that the PE coatings maintain phase stability-often retaining tetragonal ZrO_2-and structural integrity without spallation or crack propagation. In contrast, uncoated Zr cladding rapidly forms thick, brittle oxide scales, undergoes accelerated hydrogen pickup, and suffers from severe embrittlement and fragmentation. The protective nature of the PE coating not only delays oxidation kinetics but also preserves the mechanical reliability of the cladding under extreme conditions. These findings support the potential application of PE technology as a surface engineering strategy to improve accident tolerance in Zr-based nuclear fuel cladding.

A comprehensive review on high performance Zr-alloy cladding materials via direct reformation of its surface via plasma electrolysis is rarely found in literature, yet it is required to provide the integrated perspective on the structural integrity and its performance respective to current demands

 DOI: https://doi.org/10.55981/urania.2025.12906

in nuclear power reactors. Accordingly, the present review systematically examines the mechanistic study underlying formation mechanisms of PE coatings and their unique microstructure and discusses how the structural integrity of PE-coated Zr alloys would exhibit high oxidation resistance mechanisms under reactor-relevant conditions.

METHODOLOGY

This review adopts a narrative approach to synthesize and critically evaluate the existing literature on the high-temperature steam oxidation resistance of Zr cladding materials subjected to PE. Unlike bibliometric analyses, which emphasize quantitative mapping of research outputs, the narrative method was chosen to enable a detailed, mechanism-focused discussion of the underlying scientific phenomena. Relevant literature was collected from major academic databases (Scopus, Web of Science, and ScienceDirect) focusing on publications from 2015 onward that addressed PE modification of Zr claddings and their steam oxidation resistance. The inclusion criteria were limited to peer-reviewed journal articles and review papers written in English that specifically addressed (i) PE treatment of Zr or its alloys, and/or (ii) the steam oxidation behavior of such treated materials at elevated temperatures. Exclusion criteria included publications that focused solely on unrelated applications of PE, or reports lacking mechanistic discussion of oxidation resistance. The selected literature was then thematically organized into two main aspects: (1) PE coating formation mechanism on Zr, and (2) oxidation resistance of PE-coated Zr at high temperature. This framework enabled a qualitative synthesis of current knowledge while highlighting areas of consensus, divergence, and remaining research gaps.

FORMATION MECHANISM OF PE-COATED Zr ALLOYS

During PE process of Zr alloys, various electrolytes such as silicate, aluminate, and phosphate can be employed, often resulting in the incorporation of Si, Al, and P into the ZrO_2-based coating [14]. However, for Al and Si, their presence is generally not a concern, as these elements are commonly used as coating materials or as alternative cladding materials themselves [8]. The surface morphology often exhibits a characteristic volcano-like structure, which is attributed to the ejection of molten oxide under the influence of high-temperature plasma microdischarges, followed by rapid quenching of the surrounding electrolyte [15]. The resulting oxide layer consists predominantly of monoclinic (m-) and tetragonal (t-) zirconia (ZrO_2) phases, with occasional formation of cubic (c-) ZrO_2. Among these three crystallographic phases of ZrO_2, the m-ZrO_2 is thermodynamically stable at ambient temperature, whereas the t- and c-ZrO_2 phases are stable at elevated temperatures. However, the extremely high plasma temperatures, which can exceed 5000 °C during the PE process, facilitate the formation of the high-temperature t- and c-ZrO_2 phases, which are retained due to the rapid cooling conditions [8], [16]. The retention of t-ZrO_2 at room temperature is facilitated by mechanisms such as the grain size effect or constraint-induced stabilization [17].

The PE coating growth on Zr involves three main mechanisms [18]. The first is anodic oxidation, which consists of electrochemical reactions occurring under a strong electric field, inducing ion migration at the metal–electrolyte interface. Zr^{4+} ions were generated at the coating/substrate interface. Zr^{4+} then reacts with OH- from electrolyte, such as when KOH or NaOH is added to electrolyte, leading to formation of a passive ZrO_2 layer on the Zr surface, as shown in reactions (1) and (2) below:

$$Zr \rightarrow Zr^{4+} + 4e^- \quad (1)$$

$$Zr^{4+} + 2OH^- + 2H_2O \rightarrow ZrO_2 + 2H_3O^+ \quad (2)$$

As the anodizing voltage increases, dielectric breakdown occurs, which is characterized by plasma microdischarges. These microdischarges generate extremely high local temperatures, representing the second mechanism of the process. Consequently, both the substrate and the oxide layer undergo melting. Liu et al. observed an oxide layer enriched with Zr, providing evidence of a significant contribution from the Zr substrate [18]. Thus, Zr originates from the substrate and oxide, while the oxygen derives from both the oxide and the electrolyte. During this stage, species from the electrolyte also participate in the oxide formation. For instance, in aluminate-

based electrolytes, aluminate ions (AlO_2^-) react with water to form hydroxyl complexes such as $Al(OH)_4^-$, as shown in reactions (3). These negatively charged anions, along with OH^- ions, migrate toward the Zr anode under the influence of the applied electric field. Upon reaching the high-temperature plasma discharge zones, these anions react with Zr^{4+} ions released from the Zr substrate, leading to the formation of a composite oxide layer consisting of ZrO_2 and alumina (Al_2O_3), as represented by reactions (4) and (5) below [19], [20]. The amorphous Al oxide was formed as a rapid-quenching product from the reaction between $Al(OH)_4^-$ ions and the plasma discharge, as represented by reaction (6) below [18].

$$AlO_2^- + 2H_2O \rightarrow Al(OH)_4^- \quad (3)$$

$$Zr^{4+} + 4AlO_2^- + 2H_2O \rightarrow ZrO_2 + 2Al_2O_3 \quad (4)$$

$$Zr^{4+} + 4Al(OH)_4^- \rightarrow ZrO_2 + Al_2O_3 + 2Al(OH)_3 + 5H_2O \quad (5)$$

$$4Al(OH)_4^- \rightarrow 2Al_2O_3 + 2OH^- + 3H_2O \quad (6)$$

The molten oxides generated by plasma discharges are ejected from the discharge channels and rapidly quenched upon contact with the electrolyte. These materials are deposited onto the coating surface, contributing to the formation of a unique microstructure. The exposed substrate subsequently undergoes repeated cycles of electrochemical passivation and plasma discharge [18]. Figures 1(a) and (b) shows a conventional morphological structure of surface and cross-sectional view of ZIRLO subjected to PE) [21]. Meanwhile, Zhang et al. reported a layered strcuture of the nanostructured Al_2O_3–ZrO_2 composite coating produced after 30 minutes of PE treatment as shown schematically in Figure 1 (c and d). The outermost surface is predominantly covered by nanoplate-like γ-Al_2O_3 grains. Beneath the surface, smaller nanoplate or needle-like γ-Al_2O_3 grains are distributed in the subsurface layer, with both their amount and crystallinity decreasing with depth.

Throughout the coating, both m-ZrO_2 and t-ZrO_2 phases are present; however, the amount of nanocrystalline t-ZrO_2 increases with distance from the substrate, while the content and grain size of m-ZrO_2 exhibit the opposite trend. The m- and t-ZrO_2 grains are embedded within an Al_2O_3 matrix, and the concentration of Al_2O_3 increases progressively from the inner layer toward the outer surface. The formation of nanoplate-like γ-Al_2O_3 is attributed to this annealing-induced abnormal grain growth.

The coating surface formed during PE includes regions of micro-arc discharges and heat-affected zones. In the later stages of the PE process, the inward growth mechanism becomes more prominent. This suggests that the inner region near the Zr substrate is newly formed, while the outer region undergoes “annealing” in the electrolyte rather than rapid growth. As a result, the aluminum oxide adjacent to the Zr substrate remains amorphous, whereas Al_2O_3 closer to the surface becomes crystalline.

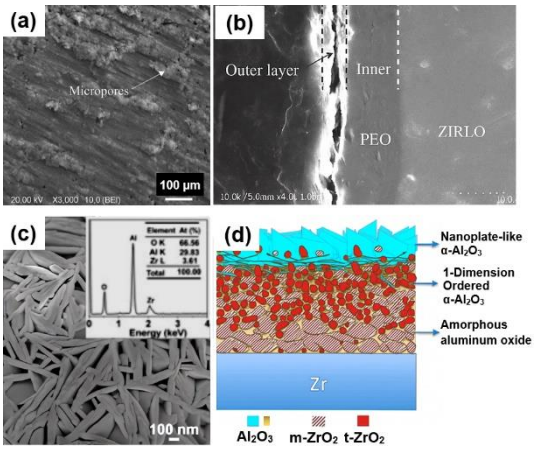

Figure 1. Morphological structure of Zr oxide on ZIRLO (a,b) [21] and a schematic diagram showing the nanoplate-like structure of PE-coated Zr in aluminate electrolyte (c,d) [17].

Additionally, Al_2O_3 plays a dual role by both suppressing the t→m transformation through constraint mechanism and inhibiting the grain growth of ZrO_2, resulting in increase of nanograin t-ZrO2 with the distance from the Zr substrate .The outer layer consists of amorphous, micrograined, and nanograined ZrO_2, with Al enrichment at grain boundaries

 DOI: https://doi.org/10.55981/urania.2025.12906

in the form of Al_2O_3. The coating growth mechanism during PE of Zr can be divided into two stages: outward and inward growth. In the initial stage, coating formation is predominantly driven by the ejection of molten oxides, resulting in outward growth. As the coating thickens, the growth mechanism transitions to inward growth, characterized by the formation of subsurface pores due to cyclic passivation and melting processes.

OXIDATION RESISTANCE AT HIGH TEMPERATURE (KINETIC AND MECHANISM)

The corrosion process of Zr alloys involves five stages [4]: water molecule dissociation, oxygen ion absorption, Zr metal oxidation, ZrO_2 formation, and hydrogen reduction. The rate of corrosion is largely determined by the migration of species such as electrons, oxygen ions, hydrogen ions, and hydroxide ions [22].

Corrosion tests for PE-coated Zr as nuclear cladding are commonly conducted in solutions containing H_3BO_3 (boric acid) and LiOH (lithium hydroxide) to simulate PWR coolant conditions. In PWR, boric acid is added to coolant to control nuclear reactivity, while LiOH serves as a pH regulator to minimize corrosion of reactor structural components and to prevent the deposition of corrosion products on the cladding surface. These aggressive ions should be prevented from penetrating the Zr substrate, and this protection largely depends on the structure and integrity of the PE coating.

The effect of the structure of PE coatings on corrosion performance has been widely studied since morphology plays a critical role in determining the coating's resistance to corrosive environments. Wang et al. reported that in PE coating formed using phosphate electrolytes, the transformation of t-ZrO_2 into m-ZrO_2 results in a porous and cracked coating [14]. Consequently, the corrosive solution can penetrate the Zr-4 substrate through localized pores and cracks in the barrier layer, leading to substrate corrosion. In contrast, PE coating in silicate electrolyte-characterized by a high content of t-ZrO_2 and a compact microstructure-offers better protection by effectively hindering the penetration of corrosive ions into the substrate. Corrosion mainly occurs due to degradation of the PE coating over prolonged exposure, which eventually leads to substrate surface exposure [14].

Corrosion tests on PE-coated Zr have also been conducted under high-temperature and/or high-pressure conditions. The application of PE coatings has been shown to reduce the reaction kinetics between Zr and steam, as evidenced by the lower weight gain observed in PE-coated samples compared to bare Zr after the test [23]. Steam oxidation of bare and PE-coated Zr at 400 °C and 10.3 MPa for up to 105 days showed that oxidation of bare Zr primarily produced m-ZrO_2, whereas the oxidation of PE-coated Zr resulted in the formation of both m-ZrO_2 and a small fraction of t-ZrO_2, whose proportion gradually decreased with increasing exposure time. The oxidation mechanism involves the dissociation of water at the oxide/water (O/W) interface, generating O^{2-} ions and protons ($2H_2O \rightarrow 4H^+ + 2O^{2-}$). The O^{2-} ions migrate from the O/W interface to the oxide/metal (O/M) interface through the grain boundaries of the PE coating, driven by both the concentration gradient and the internal electric field. At the O/M interface, O^{2-} reacts with Zr^{4+} to form ZrO_2. Due to the high Pilling–Bedworth ratio of Zr, significant compressive stress builds up, leading to the formation of metastable t-ZrO_2. As local stress continues to accumulate and reaches a critical level, microcracks are initiated, releasing stress. This stress relief facilitates the transformation of t-ZrO_2 into a more stable m-ZrO_2, particularly near crack regions. This phase transformation is accompanied by a 3–5% volume expansion, which further contributes to the cracking of the oxide layer and the progressive reduction of the t-ZrO_2 phase [23]. It is worth noting that reducing oxygen vacancies may potentially restrain the diffusion of oxygen ions, thereby lowering the corrosion rate, as observed with the addition of Nb or Ge in Zr metals [24], [25], [26].

Wang et al. conducted high temperature oxidation of bare and PE-coated Zr-1Nb alloy from 900 to 1200°C. They suggested that the high-temperature steam oxidation rate of Zr alloys is influenced not only by the phase transformation behavior of ZrO_2, the oxide grain size, and the extent of hydrogen absorption, but also by the diffusion coefficient of oxygen [27] as shown in Figure 2. As the steam oxidation temperature increases, the oxygen diffusion coefficient

also rises, resulting in a higher mass gain in both samples. Notably, the diffusion coefficient of oxygen in metallic Zr is greater than that in ZrO_2, as provided by Uetsuka et al. as follow [28] based on Arrhenius equation:

$$K = A\, e^{-\frac{B}{RT}} \quad (7)$$

$$D_{Zr} = 0.0263 \exp(-28200/RT) \quad (8)$$

$$D_{Zr(O)} = 3.923 \exp(-51000/RT) \quad (9)$$

$$D_{ZrO_2} = 0.1387 \exp(-34680/RT) \quad (10)$$

D represents the oxygen diffusion coefficient (cm²/s) over the temperature range of 1000–1500°C, R is the universal gas constant (1.987 cal·mol⁻¹·K⁻¹), and T denotes the oxidation temperature in Kelvin (K). In bare Zr, oxygen can rapidly diffuse into the substrate, causing a sharp increase in mass gain until a critical threshold is reached. Once a thick ZrO_2 layer forms on the surface, the rate of mass gain begins to decline with continued oxidation time [27].

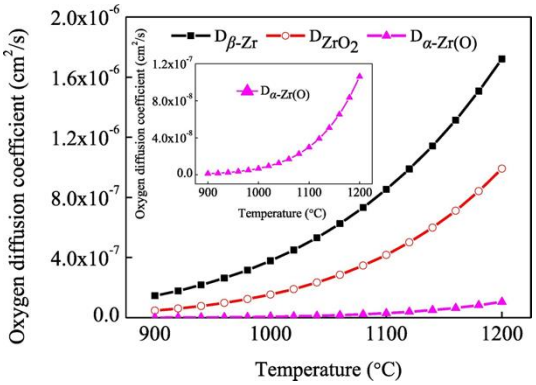

Figure 2. Oxygen diffusion coefficient of Zr, Zr(O), and ZrO_2 [27]

In the case of PE-coated Zr, the oxide layer suppresses oxygen diffusion due to its relatively low diffusion coefficient. However, at elevated temperatures of 1100 °C and 1200 °C, the PE coating is degraded by significant thermal and growth stresses. The formation of a thick oxide layer beneath the PE coating further increases internal stress. Additionally, the volume expansion associated with steam oxidation induces high compressive stress in the ZrO_2 layer, attributed to the high Pilling–Bedworth ratio of ZrO_2/Zr (1.56). This stress leads to microcrack formation and surface degradation of the PE coating. Consequently, the protective function of the PE coating against steam oxidation is largely lost at temperatures above 1100 °C. After 3600 seconds of steam exposure at 1200 °C, the final mass gains of bare and PE-coated Zr alloys become nearly identical [27].

In high-temperature corrosion studies of Zr alloys, the oxidation kinetics are commonly modeled using the equation [21], [27], [29]:

$$(\Delta W/A)^n = Kt \quad (11)$$

ΔW/A is the mass gain per unit area (mg/cm²), calculated from this equation; n is the oxidation rate exponent, *K* is the rate constant influenced by temperature and material properties, and *t* is the oxidation time in seconds. This equation serves as a powerful tool to quantify the oxidation rate under varying steam conditions, to identify the breakdown of the protective oxide layer (evident from a transition from parabolic to linear kinetics), to fit experimental data and extract kinetic parameters, and to evaluate critical thresholds of steam concentration and flow rate for ensuring safe cladding performance.

To describe the temperature dependence of the oxidation rate constant K for PE-coated Zr alloy during high-temperature steam exposure, the Arrhenius equation is employed. By fitting experimental data obtained from oxidation tests at various temperatures the authors determined the pre-exponential factors A and B. Incorporating these values into the Arrhenius model allows for the prediction of oxidation kinetics across a range of temperatures without requiring extensive experimental testing.

The corrosion resistance of the PE-coated Zr has been evaluated under a nitrogen atmosphere, revealing linear oxidation kinetics (n = 1). Despite exhibiting the same kinetic order as the bare Zr, the PE-coated samples showed a considerably lower mass gain rate, indicating improved oxidation resistance due to the protective characteristics of the coating [21]. Guan et al, as shown in Figure 3 (a), demonstrated that oxidation of PE-coated Zr alloy at 1000 °C under sufficient steam supply (without steam starvation), the oxidation follows a parabolic law with n = 2, indicating diffusion-controlled kinetics and a stable protective oxide layer [29]. After 2000 s, breakaway oxidation occurred, indicated by rapid increase in mass

 DOI: https://doi.org/10.55981/urania.2025.12906

gain rate. Breakaway oxidation occurs when the compressive stress in the oxide layer causes the mechanical break of the oxide layer. The PE coating significantly prolongs the onset of breakaway oxidation, delaying it to 1800 s compared to 1200 s for the bare Zr substrate at 1000 °C under 50% steam [21]. The oxidation kinetics of bare Zr follow a parabolic rate law (n = 2), indicating diffusion-controlled behavior. In contrast, the PE-coated sample exhibits a lower exponent (n = 0.5), suggesting a more protective oxide layer, as depicted in Figure 3 (b) and (c). However, after the onset of breakaway oxidation, both bare and PE-coated show a linear mass gain (n=1) [21]. The mechanism was proposed in Figure 4.

In bare Zirlo alloy, the diffusion of oxygen into the substrate occurred in the beginning to form an oxygen- stabilized a-Zr(O) which is then oxidized to form ZrO_2. As the ZrO_2 thickens, it further slows oxygen diffusion, leading to parabolic mass gain behavior in the pre-transition stage. While during the pre-transition stage nitrogen plays a minimal role, In the post-transition stage, limited oxygen availability near the metal-oxide interface creates Nitrogen rich conditions, facilitating formation of ZrN. This ZrN is further oxidized into ZrO_2. The repeated formation and oxidation of ZrN leads to corrosion, resulting in a linear mass gain. In the case of PE-coated Zirlo, a compact structure of PE layer initially suppresses oxygen ingress, delaying the formation of a-Zr(O) and ZrO_2 which cause earlier oxygen lacking at the interface. This promotes earlier ZrN formation compared to bare Zirlo alloy. The re-oxidation of ZrN to ZrO_2 also occurs, but both O and N diffusion remain limited by the protective PE layer, leading to a slower initial mass gain with parabolic kinetics. In the post- transition stage, although a porous ZrO_2/ZrN ZrN layer develops, the PE layer continues to act like a barrier, maintaining a lower and more stable corrosion rate than that in bare Zirlo alloys. Thus, the oxidation follows a linear trend but with delayed transition and improved resistance.

In addition to water, the addition of LiOH and H_3BO_3 also affects the corrosion of Zr. Wei et al. reported that LiOH significantly accelerates the corrosion rate of Zr alloy during autoclave corrosion test in 300 °C and 14 MPa [30]. In bare Zr, the thickness of the passive oxide layer increases with rising LiOH concentration. However, PE-coated samples exhibit lower weight gain under the same conditions. They further investigated the mechanism by which, in alkaline solutions containing OH^-, both the PE surface and the passive oxide layer acquire a negative charge, promoting the diffusion and incorporation of Li^+ ions into the oxide. These Li^+ ions can substitute for Zr^{4+} in the lattice, increasing the concentration of oxygen vacancies and thereby enhancing O^{2-} diffusion.

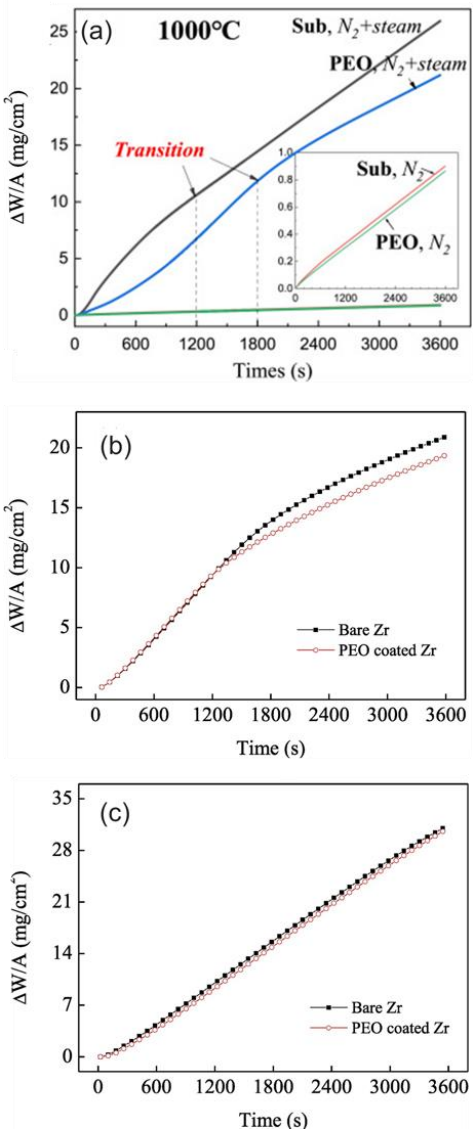

Figure 3. Kinetic oxidation of bare Zr and PE-coated Zr alloys under steam oxidative environment at (a) 1000°C [21], (b) 1100°C, and (c) 1200°C [27].

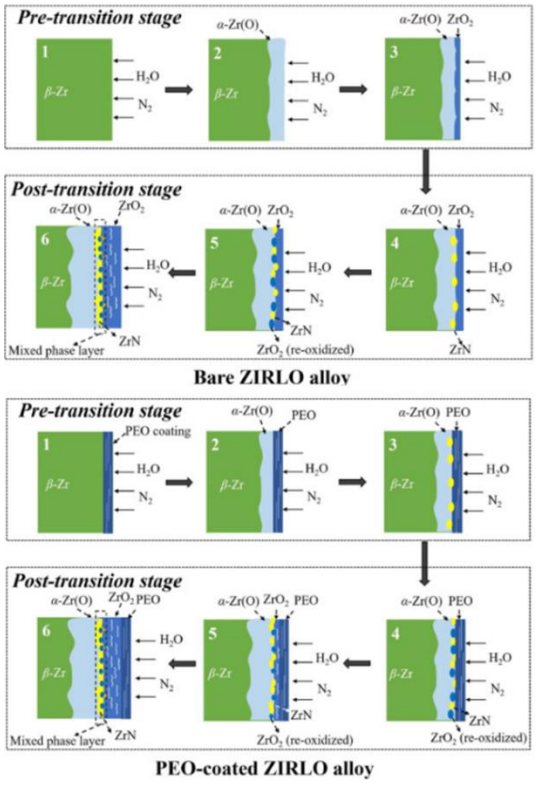

Figure 4. Schematic diagrams of the corrosion mechanisms for bare ZIRLO alloy (a) and PE-coated ZIRLO alloy in the N_2 + steam environment at temperatures above 900 °C [21].

The PE coating typically exhibits a higher (more negative) zeta potential, which may reduce the adsorption of Li^+ ions [31]. However, the presence of pores and microcracks on the PE surface facilitates Li^+ penetration into the porous outer layer. Despite this, Li^+ ions are largely retained within the PE coating and are prevented from reaching the substrate due to the presence of the dense inner barrier layer [30].

A similar observation was reported by Jiang et al. who conducted an autoclave corrosion test of ZrO_2-coated Zr4 in water at 360°C and 18.5 MPa under varied LiOH concentrations [22]. In pure water and in solutions with low LiOH concentrations, pitting corrosion was the predominant form of localized attack, and the ZrO_2 coating offered effective protection for the underlying substrate. The corrosion resistance of the coating under low LiOH conditions is influenced by several factors, including the progression of pitting corrosion, increased Li^+ ion penetration, short-circuit diffusion of O^{2-} ions, and phase transformation of ZrO_2. However, in solutions containing highly concentrated LiOH, coating degradation is primarily attributed to intergranular corrosion, internal oxidation, and through-thickness perforation caused by the ingress of LiOH [22]. Jiang reported that a higher concentration of oxygen vacancies contributes to increased tetragonality of ZrO_2 caused by ingress of LiOH [22]. This phenomenon arises because Li^+ incorporation into the ZrO_2 lattice acts as a dopant, promoting oxygen vacancy formation that stabilizes the metastable tetragonal phase. However, excess oxygen vacancies, especially near grain boundaries, facilitate microcrack formation and localized stress accumulation, ultimately weakening the structural integrity of the coating. Additionally, the chemical adsorption of water generates OH^- species that attack Zr–O–Zr bonds, promoting Zr–OH formation and inducing lattice strain, which accelerates the t- to m-ZrO_2 phase transformation and compromises coating protectiveness. The top image in Figure 5(a) illustrated that OH^- accumulation enhances Li^+ permeation into the ZrO_2, where it enables rapid O^{2-} diffusion via oxygen vacancies. This creates a micro-battery between the negatively charged, activated pit interior and the positively charged, passivated exterior, accelerating corrosion and coating dissolution. Unlike on bare Zry-4, the t-ZrO_2 phase stability here is governed by compressive stress from coating thickness, not oxygen vacancy concentration. As illustrated schematically in the bottom image of Figure 5(a), the OH^- also interacts with oxygen vacancies in t-ZrO_2, annihilating them and generating tensile stress, which further encourages t → m transformation. As the grain size of t-ZrO_2 increases beyond ~30 nm, especially under prolonged exposure, the stability of the tetragonal phase declines due to surface energy considerations, leading to phase degradation. These mechanisms promote potential differences across regions with different crystallinity, initiating pitting corrosion that evolves into deep microcracks and pore networks. At higher LiOH concentrations (e.g., 500 ppm), Li^+ and OH^- penetrate deeper into the coating, inducing oxidation stress and mismatch-related thermal expansion stress, which results in

 DOI: https://doi.org/10.55981/urania.2025.12906

interfacial debonding and severe through-thickness corrosion. Under combined effect of electrochemical and chemical reactions, when the outward diffusion of metal ions exceeds the inward diffusion of O^{2-}, some net metal fluxes are generated, releasing Zr to the coating surface to form flocculent ZrO_2 shown in the surface morphologies at the bottom image of Figure 5. Ultimately, the formation of micro-galvanic cells between active pit regions and passive surrounding areas, aided by the hydrophilic nature of ZrO_2, accelerates localized corrosion and leads to a loss of the protective function of the coating.

DISCUSSION

PE and PVD provide distinct advantages as surface modification techniques for zirconium alloys. PVD generally produces a dense and uniform layer that effectively serves as a barrier against oxidation, yet its limited wear resistance can restrict long-term mechanical durability. In contrast, PE coatings exhibit inherently high wear resistance due to their thick, hard ceramic oxide layer, with the added advantage that their porous structure can be further modified through pore filling to tailor functional properties. Despite these structural and mechanical differences, the overall weight gain observed during high-temperature oxidation tests is generally comparable between PVD- and PE-coated samples, indicating similar performance in terms of oxidation kinetics. Table 1 summarizes the results of high-temperature oxidation tests of Cr and PE coatings on Zr-based alloys.

Since neutronic economy is also a vital consideration for fuel cladding, the influence of such a coating on neutron absorption must be carefully evaluated. The ZrO_2 layer imposes a negligible neutronic penalty because oxygen possesses an exceptionally low thermal neutron absorption cross section (0.00019 barn), which is orders of magnitude lower than that of Zr itself (0.18 barn) and markedly lower than key alloying elements in Zr alloys, such as Cr (3.05 barn), Fe (2.56 barn), Sn (0.63 barn), and Nb (1.1 barn) as well as other common coating elements like Si (0.16 barn) [8]. This ensures that a pre-formed oxide layer does not significantly absorb neutrons or impair reactor efficiency.

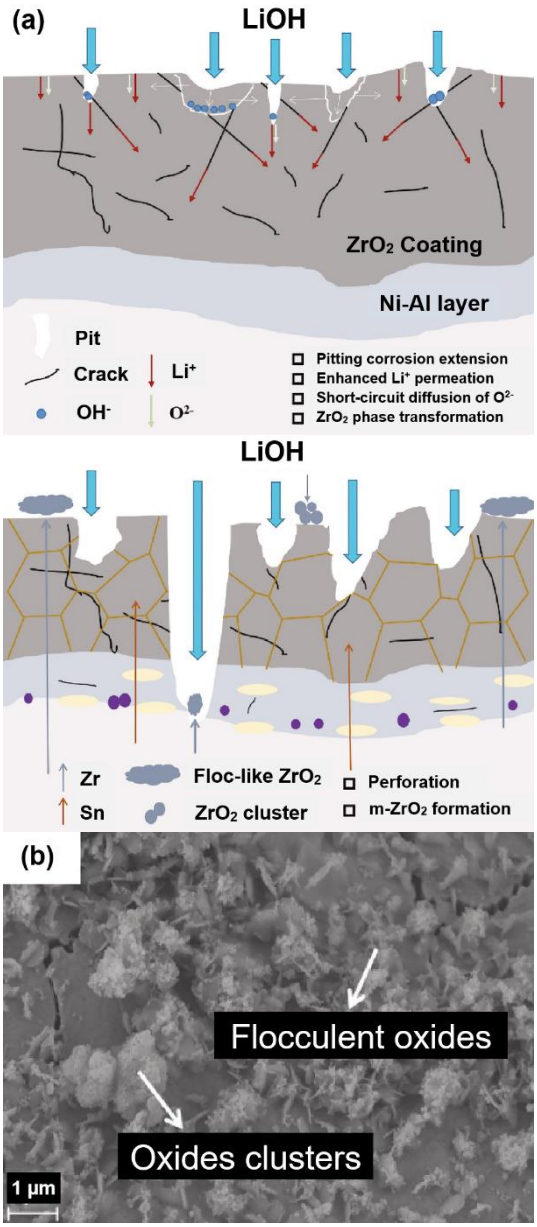

Figure 5. Schematic on corrosion process of ZrO_2 coating on Zry-4 in lithiated water (a), and representative morphologies of ZrO_2 with 500 ppm LiOH at 360 °C/18.5 MPa for 100 h (b) [22].

In addition to its neutronic transparency, the irradiation response of ZrO_2 coatings must be assessed to ensure their long-term protective performance under reactor-relevant conditions. Hu et al., who conducted a detailed microscopy study on Zr-1.0Nb alloys exposed to both autoclave oxidation and in-reactor neutron irradiation conditions (fast neutron fluence of

4.35 × 1025n/m2, E > 1 MeV), reported that under neutron irradiation the Zr oxide remains protective and does not show evidence of radiation-enhanced corrosion after ~5 dPa exposure [45]. Liu et al. investigated the effect of 500 keV He^+ ion irradiation on Al_2O_3–ZrO_2 ceramic composites at fluences up to 4.0 × 10^{17} ions/cm^2 and found that ZrO_2 exhibits higher irradiation resistance than Al_2O_3 [46]. At room temperature, irradiation induces lattice strain, volume swelling, and defect accumulation, with He bubbles evolving into ribbon-like structures and eventually microcracks at higher fluence, leading to reductions in hardness and elastic modulus. While Al_2O_3 suffers pronounced degradation, ZrO_2 limits amorphization and maintains structural stability even under high fluence. At elevated temperature (500 °C), partial recovery of irradiation-induced defects and an irradiation-assisted m- to t- transformation in ZrO_2 improve radiation tolerance. Thus, the primary degradation mechanism is linked to the bubble growth and crack propagation, but ZrO_2's resistance and high-temperature recovery effects enhance the overall radiation tolerance of the composite.

Table 1. Summary of high temperature oxidation test of Cr and PE coating for Zr-based alloys.

Coating material	Coating method	As-deposited coating thickness	High temperature oxidation test	Weight gain	Oxidation performance remarks	Ref
Cr	Magnetron sputtering	18 µm	Steam, 1200 °C (up to 240 min) and 1300 °C (up to 60 min)	-	Cr-coated samples showed much lower oxidation rates compared to uncoated zirconium, primarily due to the formation of a dense and adherent Cr_2O_3 layer that effectively suppressed oxygen diffusion. Cr–Zr diffusion layer formed at Cr and Zr interface.	[32]
Cr	Magnetron sputtering	13 µm	Steam, 1200 °C, 30–180 min	28.158 mg/cm^2	The Cr layer was initially able to protect the Zr substrate by forming Cr_2O_3, which functions as a barrier to oxygen diffusion. However, after an oxidation time of about 1.5 hours at 1200°C, the coating began to fail due to the redox reaction between Cr_2O_3 and Zr forming ZrO_2 within the layer, allowing oxygen to penetrate to the substrate. This is indicated by a change in oxidation kinetics from parabolic (slow) to linear (fast), although the overall oxidation weight remains much lower than the sample without coating.	[33]
Cr	Multi cathode and hot target magnetron sputtering	Dense 4.5 µm – and columnar 9 µm	Steam, 900 °C (30 min); 1050 °C (20 min); (1200 °C (10 min)	4.13 – 22.90 mg/cm^2	A thick columnar Cr coating fully protects Zr from oxidation at 1200 °C for 10 min, with thicker coatings offering a longer O diffusion paths during Cr consumption by Cr-Zr interdiffusion, while at lower temperatures protection depends on the dense microstructure of intact Cr layers.	[6]
Cr	Multi cathode and hot target magnetron sputtering	Dense and columnar 4.5 µm; 6 µm; and 9 µm	Steam, 1400 °C, 5 min	25.0 – 28.4 mg/cm^2	O and Cr-Zr interdiffusion consume the coatings, with columnar structures showing lower oxidation activation energi. Columnar coatings stabilize α-Zr by oxygen, slowing interdiffusion and maintaining residual Cr. At ≥1330 °C, rapid Cr-Zr interdiffusion fully consumes the coating, leading to direct Zr oxidation with α-Zr(O), ZrO_2 growth, and Cr diffusion into β-Zr.	[34]
Cr	High power impulse magnetron Sputtering	14.8 – 22.5 µm	Steam; 1200 °C; 60, 120, 240 min	-	The compact columnar Cr coatings form a thicker, dense Cr_2O_3 layer with fewer pores and cracks, which over time is reduced as Zr diffuses outward, consuming Cr_2O_3 and forming sub-surface Cr and ZrO_2.	[35]
Cr	Radio frequency magnetron sputtering	27 µm	Steam; 1200 °C; 60 and 120 min.	-	A dense Cr_2O_3 layer serves as an effective O diffusion barrier, protecting Zr-4 substrates during air oxidation at 1000 °C and steam oxidation at 1200 °C.	[36]
Cr	Arc ion plating	10 µm	Steam; 1200 °C; 33.3 min	12 mg/cm^2	Cr coating remained adherent without spallation, forming a protective Cr_2O_3 surface and Cr-Zr interdiffusion layer that suppressed α-Zr(O) and ZrO_2 growth, thereby retaining ductility under LOCA conditions.	[37]

 DOI: https://doi.org/10.55981/urania.2025.12906

Coating material	Coating method	As-deposited coating thickness	High temperature oxidation test	Weight gain	Oxidation performance remarks	Ref
Cr	Arc ion plating	15.8 µm	1200 ◦C for 30 –180 min	6 – 29 mg/cm^2	The bias voltage during deposition governs the initial microstructure of Cr coatings, which in turn controls oxidation resistance at 1200 °C steam. Optimal bias (50–100 V) produces defect-free columnar grains and a stable $ZrCr_2$ layer, enabling rapid grain growth and reduced weight gain during high-temperature oxidation.	[38]
Cr	Multi-arc ion plating	14.5 – 15.6 µm	Steam, 800, 1000 and 1200 ◦C for 120 min	-	Cr coatings produced by multi-arc ion plating exhibited superior oxidation resistance compared to Zr-4, but columnar grains with strong (001) texture accelerated oxygen diffusion and degraded stability at 1200 °C. In contrast, equiaxed grain coatings formed compact and uniform oxide films, providing the best oxidation resistance.	[39]
Cr	Cold spray	12.6 – 51 µm	Air; 1200 & 1300 °C; 3,10,20 min	-	Excellent adhesion, remaining intact after thermal cycling. Oxidation produced a thin and dense Cr_2O_3 scale that served as an effective oxygen barrier. Cr-Zr inter-diffusion layer between the Cr coating and the Zr substrate.	[40]
Bilayer Cr/Mo	Multi chatode magnetron sputtering	11 µm	Steam; 1200 °C (16.7–33.3 min), 1330 °C (2–6 min), 1400 °C (2 min)	1.51–10.09 mg/cm^2	At 1200–1330 °C, Cr-Mo bilayer coating shows better oxidation resistance than Cr single layer due to the Mo sublayer acting as a diffusion barrier. At 1400 °C for 120 s, Cr-Mo-coated samples has comparable weight gain with Cr, with eutectic Cr–Zr(Mo) interdiffusion and Mo diffusion indicating loss of barrier properties.	[41]
CrSi	Magnetron sputtering	15.4 µm	Steam, 1200 °C, 60–240 min	-	The $Cr_{0.92}Si_{0.08}$ coating exhibits superior oxidation resistance compared to pure Cr due to the formation of a protective SiO_2 sublayer that suppresses O inward and Cr outward diffusion. In-situ formation of a Zr_2Si diffusion barrier prevents Cr–Zr interdiffusion.	[42]
ZrO_2	PE	9 - 10 µm	Pure N_2 & 50% N_2+50%; 900 & 1000 °C; 60 min	-	PE coatings improve the oxidation and nitridation resistance of ZIRLO, particularly at 900 °C in N_2+steam, where the mass gain was reduced to about 55% of the bare alloy. While PE coating delayed degradation and altered corrosion kinetics, its protective effect decreased at 1000 °C due to the formation of thicker ZrO_2–ZrN layers and phase separation	[21]
ZrO_2	PE	8 µm	Steam; 900-1200 °C, 60 min	1.25-30.56 mg/cm^2	PE coating effectively improves steam oxidation resistance up to 1000 °C, but loses its protective function above 1100 °C due to coating degradation, making it useful mainly at intermediate rather than extreme high temperature	[27]
ZrO_2	PE	7 µm	Steam+Ar; 1000 and 1200 °C, 60 min	4.3-31.0 mg/cm^2	The PE coating remained intact after 3600 s testing in steam at 1200°C. Oxidation at high temperatures caused the growth of a very thick oxide layer, and the thickness of the oxide layer could reach approximately 175 µm depending on the test conditions.	[29]
ZrO_2 + Cr	PE + Vacuum Arc Deposition	16.3 µm	Steam, 1200 °C, for 60 min	14.87 mg/cm^2	PE interlayer beneath the Cr coating effectively suppresses Cr–Zr interdiffusion and reduces the formation of brittle $ZrCr_2$ phases, significantly enhancing the oxidation resistance of Zr–1Nb alloys. The PE/Cr composite coating demonstrates superior protective performance compared to either PEO or Cr coatings alone.	[43]
ZrO_2 + CrAlSi	PE + Vacuum Arc Deposition	9.5 µm	Steam, 1000 ◦C, 1100 ◦C and 1200 ◦C, 60 min	2.54 - 17.69 mg/cm^2	The PE/CrAlSi composite coating significantly enhances the oxidation resistance of Zr–2 alloy at 1000–1100 °C by forming protective oxide layers and diffusion barriers but at 1200 °C the coating is fully consumed, leading to Cr diffusion and precipitate formation in the substrate.	[44]

In addition to irradiation resistance, the ability of PE-derived ZrO_2 coatings to withstand repeated thermal cycling is crucial for ensuring their reliability under reactor transients and accident conditions. Apelfeld et al. investigated thick PE coatings (>100 μm) formed on Zr and Zr-1%Nb alloys and evaluated their behavior under high-temperature cyclic loading using a nitrogen plasmatron at surface temperatures approaching 2000 K [47]. After 63 heating–cooling cycles, the coatings retained their microstructural integrity, showing only minor surface roughening and microcrack formation. Remarkably, the thermal conductivity of the PE coatings was found to be as low as ~0.2 W/m·K at 1600 K, which is several times lower than that of reference yttria-stabilized zirconia, making them highly effective as thermal barrier layers. These findings highlight that PE coatings can sustain harsh thermal gradients while maintaining structural stability, an essential attribute for advanced fuel cladding applications.

Another critical challenge for fuel cladding in pressurized water reactors is fretting wear, which arises from the relative motion between fuel rods and structural components under coolant flow–induced vibration [48]. Excessive fretting can lead to cladding wall thinning, breach formation, and subsequent fuel failure. The hard and dense ceramic surface generated by the PE process provides superior resistance to fretting wear compared to bare Zr alloys, owing to its significantly higher hardness, lower coefficient of friction, and improved surface stability under cyclic mechanical loading. Previous tribological studies of PE coatings on Zr and other valve metals have demonstrated a substantial reduction in wear rate and material loss under simulated contact conditions. The friction coefficient can be further reduced when the pores are impregnated with nanoparticles that acts as lubricant [13], [48], [49]. These attributes suggest that PE-derived ZrO_2 coatings could serve as an effective barrier against fretting-induced degradation, thereby extending cladding lifetime and enhancing fuel reliability in reactor environments.

CHALLENGES AND FUTURE RESEARCH DIRECTION

Despite significant progress in PE coatings for Zr alloys, critical research gaps remain in understanding their long-term phase stability under cyclic thermal-mechanical stresses and performance in PWR environments. A first challenge lies in controlling the maximum coating thickness to ensure sufficient oxidation resistance without impairing the overall thermal conductivity of the cladding. Furthermore, the coating must retain good ductility and strong adhesion to the substrate, sustaining mechanical integrity during pellet–cladding mechanical interaction (PCMI) and high-temperature ballooning events. Future work should establish the maximum PE coating thickness that does not compromise the cladding's ductility and resistance to PCMI.

Although several studies have investigated the irradiation response of Zr oxides and related ceramic systems under neutron and He ion irradiation, they primarily focus on naturally formed corrosion oxides or bulk ceramic composites [45], [46], [50]. These works provide valuable insight into irradiation-induced microstructural evolution, such as defect accumulation, phase stability, swelling, and mechanical degradation of ZrO_2-based systems. However, they cannot directly represent the response of PE-formed oxide coatings under neutron irradiation. PE coatings differ fundamentally from thermally grown oxides or bulk ceramics in terms of microstructure, porosity, phase composition, and residual stress state. The PE process typically produces a heterogeneous oxide layer comprising crystalline m-, t-, or c-ZrO_2 phases intermixed with amorphous regions, pores, and cracks. These features are absent in dense bulk ceramics or corrosion-grown oxides and may serve as sinks or accelerators for irradiation-induced defect migration, He bubble formation, and stress localization. Furthermore, the layered architecture of PE coatings—with dense inner barriers and porous outer regions—could lead to distinct irradiation pathways compared with uniform oxide films. Because of these intrinsic differences, extrapolating the irradiation behavior of corrosion oxides or bulk ZrO_2 ceramics to PE coatings is insufficient. A systematic understanding of how neutron irradiation modifies the microstructure, defect chemistry, and protective properties of PE coatings is therefore essential. This knowledge is particularly critical for evaluating their performance in advanced nuclear reactor environments, where prolonged neutron exposure and high-temperature conditions prevail. Without such dedicated studies, the

 DOI: https://doi.org/10.55981/urania.2025.12906

reliability of PE-coated claddings as accident-tolerant fuel candidates cannot be fully assessed.

Additional key challenges include preventing detrimental to m-ZrO_2 phase transformations under irradiation and ensuring uniform protection across the cladding surface. Future research may develop advanced electrolyte formulations and hybrid systems to enhance the stability of PE-coated Zr alloy in aggressive environments, particularly in high-LiOH conditions. In addition, *in-situ* monitoring studies and computational modelling of stress evolution also can be elaborated to predict material degradation mechanisms, with particular emphasis on simulating crack initiation and propagation under both operational and accident conditions. Addressing these challenges through multidisciplinary approaches will be essential for advancing PE-coated Zr claddings in next-generation nuclear reactors, improving safety and performance under extreme operating conditions.

CONCLUDING REMARKS

Plasma electrolytic coatings significantly enhance Zr alloy corrosion resistance through unique microstructural characteristics, including gradient Al_2O_3 distribution and metastable t-ZrO_2 stabilization, which is strongly influenced by electrolyte composition, with silicate-based coatings outperforming phosphate ones in PWR conditions.

High-temperature steam oxidation studies confirm that PE coatings delay breakaway oxidation and reduce reaction kinetics compared to bare Zr, though the underlying mechanisms remain governed by oxygen diffusion and stress accumulation.

Environmental factors critically determine coating durability, with boric acid providing synergistic protection by pore-blocking while LiOH accelerates degradation via intergranular corrosion, internal oxidation, and through-thickness perforation due to Li^+ and OH^- penetration, oxygen vacancy formation, and phase transformation.

AUTHORIZED CONTRIBUTOR

N.N.: Conceptualization, literature study, writing-original draft-review-editing; C.K.M.: literature study; A.R.S.: literature study; J.C.S.: conceptualization, literature study, writing-review-editing, supervision

REFERENCES

[1] A. T. Motta *et al.*, “Hydrogen in zirconium alloys: A review,” *Journal of Nuclear Materials*, vol. 518, pp. 440–460, May 2019, doi: 10.1016/J.JNUCMAT.2019.02.042.

[2] Z. Cui *et al.*, “Role of microchannels in breakaway oxidation of Zr alloy under high-temperature steam oxidation at 1000 ℃,” *Corros Sci*, vol. 199, p. 110204, May 2022, doi: 10.1016/j.corsci.2022.110204.

[3] T. R. Allen, R. J. M. Konings, and A. T. Motta, “Corrosion of Zirconium Alloys,” in *Comprehensive Nuclear Materials*, Elsevier, 2012, pp. 49–68. doi: 10.1016/B978-0-08-056033-5.00063-X.

[4] A. T. Motta, A. Couet, and R. J. Comstock, “Corrosion of Zirconium Alloys Used for Nuclear Fuel Cladding,” *Annu Rev Mater Res*, vol. 45, no. 1, pp. 311–343, Jul. 2015, doi: 10.1146/annurev-matsci-070214-020951.

[5] S. J. Zinkle, K. A. Terrani, J. C. Gehin, L. J. Ott, and L. L. Snead, “Accident tolerant fuels for LWRs: A perspective,” *Journal of Nuclear Materials*, vol. 448, no. 1–3, pp. 374–379, May 2014, doi: 10.1016/j.jnucmat.2013.12.005.

[6] E. B. Kashkarov, D. V. Sidelev, M. S. Syrtanov, C. Tang, and M. Steinbrück, “Oxidation kinetics of Cr-coated zirconium alloy: Effect of coating thickness and microstructure,” *Corros Sci*, vol. 175, p. 108883, Oct. 2020, doi: 10.1016/j.corsci.2020.108883.

[7] N. M. A. Mohamed, “Cladding of nuclear fuel with iron based alloy: Penalty and solution,” *Progress in Nuclear Energy*, vol. 165, p. 104931, Nov. 2023, doi: 10.1016/j.pnucene.2023.104931.

[8] C. Tang, M. Stueber, H. J. Seifert, and M. Steinbrueck, “Protective coatings on zirconium-based alloys as accident-Tolerant fuel (ATF) claddings,” *Corrosion Reviews*, vol. 35, no. 3, pp. 141–165, Aug. 2017, doi: https://doi.org/10.1515/corrrev-2017-0010.

[9] F. Al Afghani and A. Anawati, “Plasma electrolytic oxidation of zircaloy-4 in a mixed alkaline electrolyte,” *Surf Coat*

Technol, vol. 426, p. 127786, Nov. 2021, doi: 10.1016/j.surfcoat.2021.127786.

[10] M. K. Ajiriyanto and A. Anawati, "Ultrasonication assisted plasma electrolytic oxidation accelerated growth of SiO2/ZrO2 coating on zircaloy-4," *Surf Coat Technol*, vol. 456, p. 129261, Mar. 2023, doi: 10.1016/j.surfcoat.2023.129261.

[11] M. K. Ajiriyanto and A. Anawati, "Optimizing additive Y2O3 concentration for improving corrosion resistance of ceramic coatings formed by plasma electrolytic oxidation on Zr-4 alloy," *J Phys D Appl Phys*, vol. 57, no. 45, p. 455207, Nov. 2024, doi: 10.1088/1361-6463/ad6d79.

[12] A. V. Apelfeld, A. A. Ashmarin, A. M. Borisov, A. V. Vinogradov, S. V. Savushkina, and E. A. Shmytkova, "Formation of zirconia tetragonal phase by plasma electrolytic oxidation of zirconium alloy in electrolyte comprising additives of yttria nanopowder," *Surf Coat Technol*, vol. 328, pp. 513–517, Nov. 2017, doi: 10.1016/j.surfcoat.2016.09.071.

[13] S. Arun, T. Arunnellaiappan, and N. Rameshbabu, "Fabrication of the nanoparticle incorporated PEO coating on commercially pure zirconium and its corrosion resistance," *Surf Coat Technol*, vol. 305, pp. 264–273, Nov. 2016, doi: 10.1016/j.surfcoat.2016.07.086.

[14] Y. M. Wang *et al.*, "Degradation and structure evolution in corrosive LiOH solution of microarc oxidation coated Zircaloy-4 alloy in silicate and phosphate electrolytes," *Appl Surf Sci*, vol. 431, pp. 2–12, Feb. 2018, doi: 10.1016/j.apsusc.2017.04.226.

[15] N. Nashrah, M. P. Kamil, D. K. Yoon, Y. G. Kim, and Y. G. Ko, "Formation mechanism of oxide layer on AZ31 Mg alloy subjected to micro-arc oxidation considering surface roughness," *Appl Surf Sci*, vol. 497, p. 143772, Dec. 2019, doi: 10.1016/j.apsusc.2019.143772.

[16] Y. Cheng, T. Wang, S. Li, Y. Cheng, J. Cao, and H. Xie, "The effects of anion deposition and negative pulse on the behaviours of plasma electrolytic oxidation (PEO)—A systematic study of the PEO of a Zirlo alloy in aluminate electrolytes," *Electrochim Acta*, vol. 225, pp. 47–68, Jan. 2017, doi: 10.1016/j.electacta.2016.12.115.

[17] L. Zhang, W. Zhang, Y. Han, and W. Tang, "A nanoplate-like α-Al2O3 out-layered Al2O3-ZrO2 coating fabricated by micro-arc oxidation for hip joint prosthesis," *Appl Surf Sci*, vol. 361, pp. 141–149, Jan. 2016, doi: 10.1016/j.apsusc.2015.11.132.

[18] L. Liu *et al.*, "Growth mechanism of plasma electrolytic oxidation coating of Zr alloys revealed by layer-specific phase analyses," *Appl Surf Sci*, vol. 702, p. 163336, Sep. 2025, doi: 10.1016/j.apsusc.2025.163336.

[19] N. Attarzadeh and C. V. Ramana, "Plasma Electrolytic Oxidation Ceramic Coatings on Zirconium (Zr) and ZrAlloys: Part I—Growth Mechanisms, Microstructure, and Chemical Composition," *Coatings*, vol. 11, no. 6, p. 634, May 2021, doi: 10.3390/coatings11060634.

[20] Y. Yan, Y. Han, and J. Huang, "Formation of Al2O3–ZrO2 composite coating on zirconium by micro-arc oxidation," *Scr Mater*, vol. 59, no. 2, pp. 203–206, Jul. 2008, doi: 10.1016/j.scriptamat.2008.03.015.

[21] H. Guan, Q. Zhou, C. Xu, X. Jin, J. Du, and W. Xue, "High-temperature degradation behavior of PEO-coated ZIRLO alloy in N2 and N2+steam environments at 900 and 1000 °C," *Journal of Nuclear Materials*, vol. 597, p. 155091, Aug. 2024, doi: 10.1016/j.jnucmat.2024.155091.

[22] G. Jiang, D. Xu, J. Liu, J. Yang, Y. Li, and W. Kuang, "Corrosion protection and failure mechanism of ZrO2 coating on zirconium alloy Zry-4 under varied LiOH concentrations in lithiated water at 360 °C/18.5 MPa," *Appl Surf Sci*, vol. 650, p. 159173, Mar. 2024, doi: 10.1016/j.apsusc.2023.159173.

[23] Z. Li, M. Zheng, Z. Yang, Q. Ren, Z. Cai, and Y. Jiao, "Characterization and corrosion behavior of plasma electrolytic oxidation coating on zirconium alloy in superheated steam condition," *Surf Coat Technol*, vol. 466, p. 129657, Aug. 2023, doi: 10.1016/j.surfcoat.2023.129657.

[24] J. Zhang, Y. Hu, L. Tu, F. Sun, M. Yao, and B. Zhou, "Corrosion behavior and oxide microstructure of Zr-1Nb- x Ge

alloys corroded in 360 °C/18.6 MPa deionized water," *Corros Sci*, vol. 102, pp. 161–167, Jan. 2016, doi: 10.1016/j.corsci.2015.10.005.

[25] O. H. Kwon *et al.*, "Short communication: 'Effect of Nb on the electrical resistivity of ZrO2 layer formed on Zr alloys,'" *Journal of Nuclear Materials*, vol. 536, p. 152202, Aug. 2020, doi: 10.1016/j.jnucmat.2020.152202.

[26] G. Jiang, D. Xu, W. Yang, L. Liu, Y. Zhi, and J. Yang, "High-temperature corrosion of Zr–Nb alloy for nuclear structural materials," *Progress in Nuclear Energy*, vol. 154, p. 104490, Dec. 2022, doi: 10.1016/j.pnucene.2022.104490.

[27] X. Wang *et al.*, "High temperature oxidation of Zr 1Nb alloy with plasma electrolytic oxidation coating in 900–1200 °C steam environment," *Surf Coat Technol*, vol. 407, p. 126768, Feb. 2021, doi: 10.1016/j.surfcoat.2020.126768.

[28] H. Uetsuka, T. Furuta, and S. Kawasaki, "Embrittlement of Zircaloy-4 due to Oxidation in Environment of Stagnant Steam," *J Nucl Sci Technol*, vol. 19, no. 2, pp. 158–165, Feb. 1982, doi: 10.1080/18811248.1982.9734128.

[29] H. Guan *et al.*, "Effects of steam concentration and flow rate on the high temperature oxidation of PEO-coated zirconium alloy at 1000 °C and 1200 °C," *Surf Coat Technol*, vol. 448, p. 128896, 2022, doi: https://doi.org/10.1016/j.surfcoat.2022.128896.

[30] K. Wei *et al.*, "Effects of Li, B and H elements on corrosion property of oxide films on ZIRLO alloy in 300 °C/14 MPa lithium borate buffer solutions," *Corros Sci*, vol. 181, p. 109216, Apr. 2021, doi: 10.1016/j.corsci.2020.109216.

[31] K. Wei *et al.*, "Zeta potential of microarc oxidation film on zirlo alloy in different aqueous solutions," *Corros Sci*, vol. 143, pp. 129–135, Oct. 2018, doi: 10.1016/j.corsci.2018.08.006.

[32] H.-B. Ma *et al.*, "Oxidation behavior of Cr-coated zirconium alloy cladding in high-temperature steam above 1200 °C," *Npj Mater Degrad*, vol. 5, no. 1, p. 7, Feb. 2021, doi: 10.1038/s41529-021-00155-8.

[33] J. Deng, D. Geng, Q. Sun, Z. Song, and J. Sun, "Steam oxidation of Cr-coated zirconium alloy claddings at 1200 °C: Kinetics transition and failure mechanism of Cr coatings," *Journal of Nuclear Materials*, vol. 586, p. 154684, Dec. 2023, doi: 10.1016/j.jnucmat.2023.154684.

[34] E. B. Kashkarov, D. V. Sidelev, N. S. Pushilina, J. Yang, C. Tang, and M. Steinbrueck, "Influence of coating parameters on oxidation behavior of Cr-coated zirconium alloy for accident tolerant fuel claddings," *Corros Sci*, vol. 203, p. 110359, Jul. 2022, doi: 10.1016/j.corsci.2022.110359.

[35] W. Wang, G. Zhang, C. Wang, T. Wang, Y. Zhang, and T. Xin, "Construction of Cr coatings with different columnar structure on Zircaloy-4 alloys to optimize the high-temperature steam oxidation behavior for accident tolerant fuel claddings," *J Alloys Compd*, vol. 946, p. 169385, Jun. 2023, doi: 10.1016/j.jallcom.2023.169385.

[36] Q. S. Chen *et al.*, "Microstructure and high-temperature steam oxidation properties of thick Cr coatings prepared by magnetron sputtering for accident tolerant fuel claddings: The role of bias in the deposition process," *Corros Sci*, vol. 165, p. 108378, Apr. 2020, doi: 10.1016/j.corsci.2019.108378.

[37] J.-H. Park, H.-G. Kim, J. Park, Y.-I. Jung, D.-J. Park, and Y.-H. Koo, "High temperature steam-oxidation behavior of arc ion plated Cr coatings for accident tolerant fuel claddings," *Surf Coat Technol*, vol. 280, pp. 256–259, Oct. 2015, doi: 10.1016/j.surfcoat.2015.09.022.

[38] T. Jung, H. Jang, Y. K. Cho, and D. Jang, "Degradation behavior of chromium-coated zirconium cladding under 1200 oC steam oxidation according to the coating microstructure," *Journal of Nuclear Materials*, vol. 603, p. 155360, Jan. 2025, doi: 10.1016/j.jnucmat.2024.155360.

[39] Y. Peng, P. Du, Y. Liu, H. Wang, S. Liu, and W. Zhang, "Investigation on Microstructures and High-Temperature Oxidation Resistance of Cr Coatings on Zircaloy-4 by Multi-Arc Ion Plating Technology," *Materials*,

vol. 15, no. 19, p. 6755, Sep. 2022, doi: 10.3390/ma15196755.

[40] B. Maier *et al.*, "Development of cold spray chromium coatings for improved accident tolerant zirconium-alloy cladding," *Journal of Nuclear Materials*, vol. 519, pp. 247–254, Jun. 2019, doi: 10.1016/j.jnucmat.2019.03.039.

[41] M. Syrtanov, E. Kashkarov, A. Abdulmenova, K. Gusev, and D. Sidelev, "High-Temperature Steam Oxidation of Accident-Tolerant Cr/Mo-Coated Zr Alloy at 1200–1400 °C," *Coatings*, vol. 13, no. 1, p. 191, Jan. 2023, doi: 10.3390/coatings13010191.

[42] S. Zeng *et al.*, "Improved oxidation resistance of Cr-Si coated Zircaloy with an in-situ formed Zr2Si diffusion barrier," *Npj Mater Degrad*, vol. 7, no. 1, p. 56, Jul. 2023, doi: 10.1038/s41529-023-00373-2.

[43] X. Wang *et al.*, "Effect of PEO interlayer on oxidation behavior of PEO/Cr composite coating on Zr–1 Nb alloy in 1200 °C steam," *Corros Sci*, vol. 226, p. 111676, Jan. 2024, doi: 10.1016/j.corsci.2023.111676.

[44] Q. Zhou *et al.*, "Effects of Al and Si elements on oxidation behavior in 1000–1200 °C steam for PEO/CrAlSi composite coating on Zr alloy," *Surf Coat Technol*, vol. 482, p. 130705, Apr. 2024, doi: 10.1016/j.surfcoat.2024.130705.

[45] J. Hu *et al.*, "Effect of neutron and ion irradiation on the metal matrix and oxide corrosion layer on Zr-1.0Nb cladding alloys," *Acta Mater*, vol. 173, pp. 313–326, Jul. 2019, doi: 10.1016/j.actamat.2019.04.055.

[46] Y. Liu *et al.*, "Irradiation response of Al2O3-ZrO2 ceramic composite under He ion irradiation," *J Eur Ceram Soc*, vol. 41, no. 4, pp. 2883–2891, Apr. 2021, doi: 10.1016/j.jeurceramsoc.2020.11.042.

[47] A. V. Apelfeld *et al.*, "The study of plasma electrolytic oxidation coatings on Zr and Zr-1% Nb alloy at thermal cycling," *Surf Coat Technol*, vol. 269, pp. 279–285, May 2015, doi: 10.1016/j.surfcoat.2015.02.039.

[48] Z. Li, Z. Cai, X.-J. Cui, R. Liu, Z. Yang, and M. Zhu, "Influence of nanoparticle additions on structure and fretting corrosion behavior of micro-arc oxidation coatings on zirconium alloy," *Surf Coat Technol*, vol. 410, p. 126949, Mar. 2021, doi: 10.1016/j.surfcoat.2021.126949.

[49] M. Karimi, M. Jafari Eskandari, and M. Araghchi, "Fabrication and characterization of graphene oxide/zirconium dioxide coatings produced by plasma electrolytic oxidation of Zr–1%Nb alloys," *Results in Surfaces and Interfaces*, vol. 14, p. 100205, Feb. 2024, doi: 10.1016/j.rsurfi.2024.100205.

[50] G. Pu *et al.*, "Effects of He ion irradiation on the microstructures and mechanical properties of t' phase yttria-stabilized zirconia ceramics," *J Alloys Compd*, vol. 771, pp. 777–783, Jan. 2019, doi: 10.1016/j.jallcom.2018.08.259.